THE JOURNAL OF BIOLOGICAL CHEMISTRY VOL. 286, NO. 52, pp. 45103–45115, December 30, 2011

The Vinculin C-terminal Hairpin Mediates F-actin Bundle Formation, Focal Adhesion, and Cell Mechanical Properties*[S]

Received for publication, April 17, 2011, and in revised form, October 27, 2011 Published, JBC Papers in Press, November 3, 2011, DOI 10.1074/jbc.M111.244293

Kai Shen[‡1,2], Caitlin E. Tolbert[§1], Christophe Guilluy[§], Vinay S. Swaminathan[¶], Matthew E. Berginski[‖], Keith Burridge[§], Richard Superfine[¶], and Sharon L. Campbell[‡**3]**

*From the Departments of [‡]Biochemistry and Biophysics, [§]Cell and Developmental Biology, [¶]Physics, and [‖]Biomedical Engineering and **Lineberger Comprehensive Cancer Center, University of North Carolina at Chapel Hill, Chapel Hill, North Carolina 27599*

Vinculin is an essential and highly conserved cell adhesion protein, found at both focal adhesions and adherens junctions, where it couples integrins or cadherins to the actin cytoskeleton. Vinculin is involved in controlling cell shape, motility, and cell survival, and has more recently been shown to play a role in force transduction. The tail domain of vinculin (Vt) contains determinants necessary for binding and bundling of actin filaments. Actin binding to Vt has been proposed to induce formation of a Vt dimer that is necessary for cross-linking actin filaments. Results from this study provide additional support for actin-induced Vt self-association. Moreover, the actin-induced Vt dimer appears distinct from the dimer formed in the absence of actin. To better characterize the role of the Vt strap and carboxyl terminus (CT) in actin binding, Vt self-association, and actin bundling, we employed smaller amino-terminal (NT) and CT deletions that do not perturb the structural integrity of Vt. Although both NT and CT deletions retain actin binding, removal of the CT hairpin (1061–1066) selectively impairs actin bundling *in vitro*. Moreover, expression of vinculin lacking the CT hairpin in vinculin knock-out murine embryonic fibroblasts affects the number of focal adhesions formed, cell spreading as well as cellular stiffening in response to mechanical force.

The ability of cells to sense and respond to environmental cues such as mechanical forces is critical for multiple cellular processes including embryogenesis and wound healing (1–3). To transmit forces across the cell membrane in both directions, the actin cytoskeleton couples transmembrane receptors (integrin or cadherin), through points of cell adhesion consisting of multiple protein complexes that form cell-extracellular matrix (focal adhesions) and cell-cell (adherens junctions) contacts (3, 4). Vinculin is an abundant protein found in both focal adhesions and adherens junctions, and plays a key role in regulating cell morphology, cell motility, and force transduction (2, 5). Vinculin is essential during development as vinculin knock-out (KO) mouse embryos fail to survive beyond day E10 with extensive defects in myocardial and endocardial structures (6). Consistent with a role in muscle structure, vinculin KO mice are predisposed to stress-induced cardiomyopathy (7). Moreover, mutations and deletions in the tail domain of metavinculin, a splice isoform of vinculin, are associated with dilated cardiomyopathy (8–10). Vinculin also possesses tumor suppressor properties as vinculin KO cells are less adherent, have a rounded morphology, reduced lamellipodial stability, increased motility (6, 11), and are resistant to apoptosis and anoikis (12).

Vinculin is a highly conserved cytoskeletal protein that has 1066 residues and contains a globular head, a flexible proline-rich linker, and a tail domain (13). Each discrete vinculin domain recognizes multiple binding partners: the vinculin head (Vh)[4] binds to talin, α-actinin, and IpaA (14–16); the proline-rich linker interacts with vasodilator stimulated phosphoprotein (VASP), CAP/ponsin, vinexin, and the Arp2/3 complex (17–20); the vinculin tail (Vt) associates with filamentous actin (F-actin), phosphatidylinositol (4,5)-bisphosphate, and paxillin (21–23). In the autoinhibitory form of vinculin, tight intramolecular interactions between Vh and Vt occlude binding to most of its ligands (13). Vinculin becomes activated upon release of autoinhibitory Vh/Vt interactions, leading to recruitment and formation of multiprotein adhesion complexes (24–27). When activated at focal adhesions (FAs) (28), vinculin serves as a mechanotransducer because it helps establish the link between membrane-associated integrins and the cytoskeleton through its association with talin and F-actin. Vinculin interacts with a number of cell adhesion proteins, acidic phospholipids, and can be phosphorylated by both tyrosine and serine/threonine kinases. However, it is currently unclear how these interactions and covalent modifications contribute to its role in regulating cell morphology, motility, and cell survival.

The structure of full-length vinculin was solved by x-ray crystallography (PDB codes 1ST6 and 1TR2), and found to possess an all helical fold (13, 29). Vinculin contains a large 90-kDa Vh domain comprised of helical bundles and is linked to Vt via a proline-rich region. The proline-rich region is likely to be unstructured and/or dynamic as it lacks electron density in the crystal structures of full-length vinculin. Vt is comprised of an

* This work was supported, in whole or in part, by National Institutes of Health Grants GM081764 (to S. L. C.), GM080568 (to S. L. C.), and GM029860 (to K. B.).

[S] The on-line version of this article (available at http://www.jbc.org) contains supplemental Figs. S1–S3.

[1] Both authors contributed equally to this work.

[2] Present address: Dept. of Natural Sciences, Savannah State University, Savannah, GA 31404.

[3] To whom correspondence should be addressed: Dept. of Biochemistry and Biophysics, CB 7260, UNC Chapel Hill, NC 27599-7260. Tel.: 919-966-7139; Fax: 919-966-2852; E-mail: sharon_campbell@med.unc.edu.

[4] The abbreviations used are: Vh, vinculin head residues 1–855; BS3, bis(sulfosuccinimidyl) suberate; CT, C-terminal; DSS, disuccinimidyl suberate; FAs, focal adhesions; F-actin, filamentous actin; FN, fibronectin; MEFs, murine embryo fibroblasts; NT, N-terminal; Vin$^{-/-}$, vinculin knock-out cells; Vt, vinculin tail residues 879–1066; HSQC, heteronuclear single quantum coherence; A/V, actin/vinculin; PDB, Protein data bank.

antiparallel 5-helix bundle that contains an N-terminal strap region (NT, residues 879–892) and a C-terminal arm (CT, residues 1051–1066) that forms interactions with the core helix bundle. The structure of the isolated Vt domain was also solved independently by x-ray crystallography (PDB code 1QKR) (30). Although the Vt domain specifically interacts with actin and acidic phospholipids, binding to these ligands is significantly reduced in the context of full-length vinculin, as intramolecular interactions between Vh and Vt partially mask their association with Vt. However, as the structure of the isolated tail domain is similar to its structure within the full-length protein, a number of studies investigating Vt/ligand interactions have been conducted using the isolated Vt domain, as this is believed to be a good model of Vt/ligand interactions that occur when Vt is freed from Vh upon activation.

Models for how Vt interacts and bundles F-actin have been proposed. For example, Johnson and Craig (31) proposed that actin association with Vt promotes a conformational change in Vt that exposes a cryptic dimerization site that promotes actin filament bundling. In a more recent study combining electron microscopy, computational docking, and mutagenesis approaches, Janssen *et al.* (32) proposed a model for the Vt·F-actin complex in which F-actin associates through two distinct binding sites on Vt, with site 1 containing residues in helices 2 and 3 of Vt and site 2 comprising a binding interface from helices 3, 4, and the CT. Moreover, results obtained from deletion mutagenesis studies indicate that the NT and CT of Vt have opposing roles in actin bundling. Although removal of the NT strap impaired actin bundling, deletion of the CT enhanced the ability of Vt to bundle actin filaments (32). However, large deletions within globular proteins can affect their structural integrity. In fact, the CT of vinculin forms contacts with both the strap and the helix bundle, and it has been previously shown that a Vt variant (Vt ΔC, 1052–1066) containing a 15-amino acid CT deletion alters NMR spectral properties, reduces stability, and makes Vt ΔC more susceptible to proteolytic degradation (33, 34).

Hence, we made smaller deletions in the NT and CT of Vt that do not significantly alter Vt structure, and have assessed actin binding and bundling properties of these mutants. Contrary to previous results, our studies indicate that the CT hairpin, rather than the NT strap is important for F-actin bundling *in vitro*. We also conducted cross-linking studies on Vt in the presence and absence of actin, and results from these studies provide additional support for formation of an actin-induced Vt dimer that is distinct from a dimer that can be formed in the absence of actin. Furthermore, we investigated the effect of vinculin CT hairpin deletion on FA morphology and mechanical properties in vinculin KO murine embryonic fibroblasts ($Vin^{-/-}$ MEFs). Our results demonstrate that deletion of the CT hairpin affects the number of focal adhesions and alters its response to mechanical forces (35).

EXPERIMENTAL PROCEDURES

Vinculin Tail Protein Expression and Purification—The tail domain of chicken vinculin (Vt) containing residues 879–1066 was cloned into a pET15b vector (Novagen, Madison, WI) (34). Several deletion variants were generated from this Vt construct, including two Vt NT strap deletions (a 5-amino acid strap deletion (884–1066 (ΔN5)) and a full strap deletion (893–1066 (Δstrap)), and three CT deletion variants (879–1061 (ΔC5), 879–1064 (ΔC2), and 879–1065 (ΔC1)). All Vt variants were generated using QuikChange site-directed mutagenesis (Stratagene, La Jolla, CA), with sequences verified by DNA sequencing. Vinculin protein expression and purification have been reported previously (34). Briefly, Vt plasmids were transformed into *Escherichia coli* strain BL21(DE3)RIPL. Cells were grown either in Lysogeny broth-rich media or M9 minimal media with $^{15}NH_4Cl$ as the sole nitrogen source at 37 °C to an A_{600} of 0.6. The cell cultures were cooled to 18 °C before adding isopropyl β-D-1-thiogalactopyranoside to a final concentration of 0.5 mM to induce Vt expression overnight. Cells were then pelleted by centrifugation at 5,800 × *g* for 30 min and re-suspended in the lysis buffer (20 mM Tris, 150 mM NaCl, 5 mM imidazole, 2 mM β-mercaptoethanol, pH 7.4) before sonication. The cell lysate was then clarified at 25,000 × *g* for 1 h, and the supernatant was loaded onto a nickel affinity column (Qiagen, Germantown, MD) and washed twice with an nickel wash buffer (20 mM Tris, 150 mM NaCl, 60 mM imidazole, 5 mM β-mercaptoethanol, pH 7.5). Histidine-tagged Vt protein was then eluted with a nickel elution buffer (20 mM Tris, 150 mM NaCl, 500 mM imidazole, 5 mM β-mercaptoethanol, pH 7.5). The His tag was removed by addition of thrombin (Sigma), and further purified by cation-exchange (Hiprep SP XL 16/10) fast protein liquid chromatography (GE Healthcare). All Vt variants were examined by SDS-PAGE gel to assess purity and protein integrity before being employed for biochemical assays.

Actin Co-sedimentation Assay—The actin binding and bundling properties of the Vt variants were assessed using an adapted actin co-sedimentation assay (36). Briefly, monomeric actin (G-actin) purified from rabbit muscle acetone powder (Pel-Freez Biologicals, Rogers, AR) was polymerized with an equal volume of 2× actin polymerization buffer (20 mM Tris, 200 mM KCl, 5 mM $MgCl_2$, 4 mM dithiothreitol (DTT), pH 7.5) at room temperature for 30 min. To assess binding of the Vt variants with F-actin, a 100-μl sample in 1× actin polymerization buffer containing actin at concentrations ranging from 0 to 60 μM and 10 μM Vt protein was incubated at room temperature for 1 h. It should be noted that the A/V ratio was determined based on the G-actin concentration, given difficulties associated with the quantifying F-actin concentration due to the heterogeneity of F-actin polymers. The samples were centrifuged at high speed (184,200 × *g*) on a Beckman-Coulter TLA 100 rotor for 30 min at 25 °C. For bundling assays, a 100-μl sample in 1× actin polymerization buffer containing 20 μM actin and 10 μM Vt protein was incubated at room temperature for 1 h. Samples containing F-actin bundles were obtained by careful extraction of the supernatant upon low speed centrifugation (5,000 × *g*). The pellet was then re-suspended in 100 μl of 0.1% SDS buffer (0.1% SDS, 25 mM glycine and 25 mM Tris, pH 8.3). Actin and Vt protein contained in both the supernatant and solubilized pellet were separated using 15% SDS-PAGE gels. Actin and Vt proteins in both samples were quantified using the densitometry software package Alpha EaseFC (Alpha Innotech, San Leandro, CA). Actin binding properties of Vt variants were calculated as follows.

$$\%\ \text{Vt binding} = \frac{\text{Vt}_{\text{denso,pellet}}}{\text{Vt}_{\text{denso,pellet}} + \text{Vt}_{\text{denso,supernatant}}} \quad \text{(Eq. 1)}$$

where $\text{Vt}_{\text{denso,pellet}}$ is the densitometry reading of Vt pelleted at 184,200 × *g*, whereas $\text{Vt}_{\text{denso,supernatant}}$ is the densitometry reading of Vt retained in the supernatant. Actin bundling properties of Vt variants were calculated as follows,

$$\%\ \text{F-actin bundled} = \frac{\text{Actin}_{\text{denso,pellet}}}{\text{Actin}_{\text{denso,pellet}} + \text{Actin}_{\text{denso,supernatant}}} \quad \text{(Eq. 2)}$$

where $\text{Actin}_{\text{denso,pellet}}$ is the densitometry reading of actin pelleted at 5,000 × *g* and $\text{Actin}_{\text{denso,supernatant}}$ is the densitometry reading of actin retained in the supernatant.

Fluorescence Microscopy of F-actin Bundles—F-actin bundles induced by the addition of WT or Vt ΔC5 were visualized using fluorescence microscopy, as previously described (36). Samples were prepared following conditions described for the actin bundling assay. Briefly, 20 μM pre-polymerized actin was incubated alone or with 10 μM Vt proteins (WT Vt or Vt ΔC5) at room temperature for 1 h. The mixture was then diluted 20 × with 1× actin polymerization buffer (10 mM Tris, 100 mM KCl, 2.5 mM $MgCl_2$, 2 mM DTT), pH 7.5. Alexa Fluoro-488 phalloidin (Invitrogen) was added to the mixture to a final concentration of 1.5 μM and then incubated for 5 min at room temperature. The sample was diluted to an actin concentration of 50 nM. Five-microliter sample aliquots were placed on a glass slide and covered with a glass coverslip. Fluorescence images were acquired on a Zeiss Axiovert 200M microscope equipped with a 60× objective lens and a Hamamatsu ORCA-ERAG digital camera.

NMR Spectroscopy—^{15}N-enriched Vt samples were exchanged into NMR buffer (10 mM potassium phosphate, 50 mM NaCl, 0.1% NaN_3, 2 mM DTT, pH 5.5) and concentrated to 0.3 mM with 10% D_2O added. Two-dimensional ^{1}H-^{15}N heteronuclear single quantum coherence (HSQC) NMR spectra were acquired on a Varian INOVA 700 MHz spectrometer at 37 °C (37). NMR data were processed with NMRPipe (38) and analyzed using NMRViewJ (39).

Circular Dichroism (CD) Spectroscopy—Both WT Vt and Vt ΔC2 were exchanged into CD buffer (10 mM potassium phosphate, 50 mM Na_2SO_4, pH 7.5). CD spectra were acquired for both far (260–190 nm) and near (350–250 nm) ultraviolet (UV) spectra regions (34) at 25 °C on an Applied Photophysics Chirascan Plus CD spectrometer. Vt variant concentrations were adjusted to 5 μM and 0.45 mM for far and near UV CD spectra acquisition, respectively.

Chemical Cross-linking of Vt Proteins—Chemical cross-linking of Vt in the presence and absence of actin was carried out using a procedure similar to that described by Johnson and Craig (31). However, instead of using disuccinimidyl suberate (DSS), bis(sulfosuccinimidyl) suberate (BS3, Thermo Scientific), a water-soluble DSS analog, was employed. In the cross-linking reactions, freshly purified Vt proteins were buffer exchanged into a cross-linking sample buffer (10 mM sodium phosphate, 100 mM NaCl, 0.02% NaN_3, pH 7.5). Actin was polymerized as described in the actin co-sedimentation assay. Vt proteins (2.5 μM) were mixed with 0–15 μM actin in the cross-linking reaction buffer (2 mM $NaHCO_3$, 100 mM NaCl, 2 mM $MgCl_2$, 0.2 mM $CaCl_2$, 0.2 mM ATP, 0.02% NaN_3, pH 7.6). Cross-linking reactions were carried out by adding BS3 to a final concentration of 25 μM. After incubation at room temperature for 40 min, the cross-linking reaction was quenched with 1 M Tris, pH 7.5, to a final concentration of 50 mM Tris. The cross-linked products were separated by either 7% NuPAGE Tris acetate gels (Invitrogen) or 15% SDS-PAGE gels followed by Western blot analysis. Vt protein bands were detected using a rabbit anti-chicken Vt antibody (31), a gift from Dr. Susan Craig (John Hopkins University), and HRP-conjugated anti-rabbit IgG (Promega, Madison, WI). Actin containing bands were detected using a rabbit anti-actin polyclonal antibody (Sigma).

Cell Culture—Vinculin-null murine embryo fibroblasts ($Vin^{-/-}$) (6) were obtained from Dr. Eileen Adamson (Burnham Institute, La Jolla, CA) and grown in Dulbecco's modified Eagle's medium (DMEM; Invitrogen) supplemented with 10% fetal bovine serum (Sigma) and antibiotic-antimycotic solution (Sigma).

DNA Constructs and Transfection—GFP-tagged full-length chicken vinculin(1–1066) plasmid in pGZ21XdZ vector was obtained from Dr. Kenneth Yamada (National Institutes of Health). The ΔC5 variant of GFP vinculin was generated using a QuikChange site-directed mutagenesis kit (Stratagene) and verified by DNA sequencing. Cells were transfected with vinculin expression constructs using Lipofectamine (Invitrogen) and Plus Reagent (Invitrogen) according to the manufacturer's protocol and examined 48 h following transfection.

Adhesion Site Analysis—Cells were seeded onto glass coverslips coated with fibronectin (FN) (50 μg/ml). After 120 min, cells were washed with phosphate-buffered saline (PBS), fixed in phosphate-buffered 4% paraformaldehyde for 15 min, permeabilized in 0.3% Triton X-100 for 10 min, blocked for 10 min in 5% bovine serum albumin, and incubated with Alexa Fluor 594-conjugated phalloidin (Molecular Probes) for 30 min. Immunofluorescence images were taken with a Zeiss Axiovert 200M microscope equipped with a Hamamatsu ORCA-ERAG digital camera and Metamorph work station (Universal Imaging Corp.). A previously described method was adapted to identify and quantify the properties of the vinculin-stained adhesions (40). This method applies a high pass filter to the images and applies a user-specified threshold to identify adhesions. We found that the watershed-based segmentation method proposed in Ref. 40 was unnecessary for our application, instead objects connected in a four-pixel neighborhood were assigned unique adhesion labels using a Matlab script recently described (41). Adhesions touching the edge of the field of view were removed and any holes in individual adhesions were filled. Finally, adhesion sizes and the number of adhesions per image were counted.

Force Microscopy—Three-dimensional force microscopy (35) was used for applying controlled and precise 60–100 piconewton local force to the magnetic beads. Tosyl-activated magnetic dynabeads (2.8 μm, Invitrogen) were washed with phosphate buffer and incubated for 24 h with FN at 37 °C. After three washes with PBS, the beads were sonicated and incubated

with cells for 40 min. Upon force application, bead displacements were recorded with high speed video camera (Jai Pulnix, San Jose, CA) and tracked using Video Spot Tracker software developed by the Center for Computer Integrated Systems for Microscopy and Manipulation at the University of North Carolina-Chapel Hill. The three-dimensional force microscopy system was calibrated prior to experiments using a fluid of known viscosity. Beads that showed displacements less than 10 nm (detection resolution of the three-dimensional force microscopy) were not selected for analysis. Custom Matlab scripts were used to calculate the creep compliance J_{max}, also referred to as deformability, which is defined as the average time-dependent deformation normalized by the constant stress applied,

$$J_{max} = \frac{r_{max}}{F \times 6\pi\alpha} \quad \text{(Eq. 3)}$$

where r_{max} is the displacement of the bead due to an applied force, F and a are the radius of the bead. Each compliance curve was then fit to a Jeffrey's (modified Kelvin-Vogit) model for viscoelastic materials (42, 43). Stiffness was reported as the value of k in pascals. Subsequent pulses were fit in the same manner and the average k for each cell type and pulse number was obtained and reported as mean ± S.E. All statistical analyses, including two-tailed Student's t test for p values, were performed in Microsoft Excel.

RESULTS

The structure of the chicken Vt domain has been solved by x-ray crystallography (30), and is comprised of a 5-helix bundle fold containing both NT and CT extensions that form contacts with the helix bundle. The NT extension (residues 879–892), termed "strap," packs against an interface formed between Vt helices 1, 2, and the CT hairpin. Johnson and Craig (31) performed chemical cross-linking studies on Vt in the absence and presence of F-actin using a Vt construct with a partial deletion in the strap (884–1066), and proposed a model in which actin binding to Vt induces a conformational change in Vt that promotes Vt dimerization and F-actin bundling. Moreover, results obtained by Janssen *et al.* (32) indicated that the strap region of Vt was important for F-actin-induced Vt dimerization, as removal of the strap (893–1066) significantly reduced actin bundling efficiency by ~60%. On the other hand, removal of 15 CT amino acids (Vt ΔC), was found to increase bundling by 23%. Based on these results, the authors suggested that the Vt CT may act to obstruct actin-mediated Vt dimer formation and actin bundling. However, the CT of vinculin forms contacts with the strap and the helix bundle, and it has been previously shown that Vt ΔC alters NMR spectral properties, reduces stability, and is more susceptible to proteolytic degradation (33, 34). As the study from Janssen and co-workers (32) focused on large deletions (13–15 amino acid) of the NT and CT of Vt that could potentially alter the structural integrity of the protein, we conducted actin binding and bundling analyses with smaller deletion variants of Vt.

Deletion of Vt Strap Does Not Affect Actin Binding and Bundling—We first compared actin bundling properties of WT Vt(879–1066) with the Vt variant that lacks the strap (Vt Δstrap, 893–1066) as well as a smaller 5-amino acid NT deletion mutant (Vt ΔN5, 884–1066). Although actin binding and bundling assays on vinculin have been reported with different actin/vinculin (A/V) molar ratios (31, 32, 36, 44), this ratio is an important consideration, because a low A/V ratio will limit the amount of the Vt dimer induced in the presence of F-actin and consequently the amount of actin bundling. Therefore, we have employed an A/V ratio in our actin bundling experiments that results in saturation or close to saturation binding of Vt to actin. According to the structure based model of the Vt·actin complex, one Vt molecule binds to two adjacent actin molecules located on the same actin filament (32). Given this model, we expect that an A/V ratio of 2 will saturate the F-actin binding sites on Vt, assuming all of the G-actin polymerizes into functional F-actin polymers. We therefore screened A/V ratios from 0.5 up to 6 while keeping the WT Vt concentration constant (10 μM), with quantification of the A/V ratio as described under "Experimental Procedures." The amount of Vt associated with F-actin at various A/V ratios is illustrated in Fig. 1*A*. Consistent with the model of Janssen *et al.* (32), we find that most of the Vt associates with F-actin at an A/V ratio of 2 (actin concentration: 20 μM), with a small increase from 60 to ~70% observed at A/V ratios of 6.

To assess the role of the Vt NT strap in actin binding, we conducted actin co-sedimentation experiments at actin concentrations of 0–30 μM and a Vt concentration of 10 μM, and compared actin binding properties of WT Vt with two NT deletion mutants, Vt ΔN5 and Vt Δstrap, with the results shown in Fig. 1. Results from these studies (Fig. 1*B*) indicate that both the partial (ΔN5) and full (Δstrap) strap deletion variants show slightly enhanced association with actin compared with WT Vt. We also examined actin bundling properties of the two NT deletion variants, at an A/V ratio of 2. As shown in Fig. 1*C*, we observe similar actin bundling efficiency for both Vt ΔN5 and Vt Δstrap compared with WT Vt. Importantly, previous work by our lab suggested that deletion of 5 NT amino acids (Vt ΔN5) from Vt does not affect the structural integrity of the Vt helix bundle (34). Taken together, these results suggest that neither a small deletion of the N terminus nor removal of the entire strap impairs actin binding or bundling, in contrast to previous findings (32).

Vt CT Deletion Mutants Are Impaired in Actin Bundling but Not Actin Binding—Studies by Janssen *et al.* (32) found that removal of 15 amino acids from the Vt CT arm (Vt ΔC) enhanced the ability of vinculin to bundle F-actin, and proposed that the Vt CT arm may require a conformational rearrangement so that it does not obstruct formation of the F-actin-induced Vt dimer. However, the Vt CT arm forms multiple interactions with the helix bundle and strap, and removal of the Vt CT arm has been shown to alter both the structural integrity and stability of the tail domain (34). In particular, our previous NMR studies indicate that deletion of 7 or more amino acids from the CT may alter the structural integrity of Vt, consistent with previous findings that Vt ΔC is highly sensitive to protease degradation (33). Therefore, we examined the effect of smaller deletions within the CT hairpin (1061–1066) on the ability of Vt to bind and bundle F-actin.

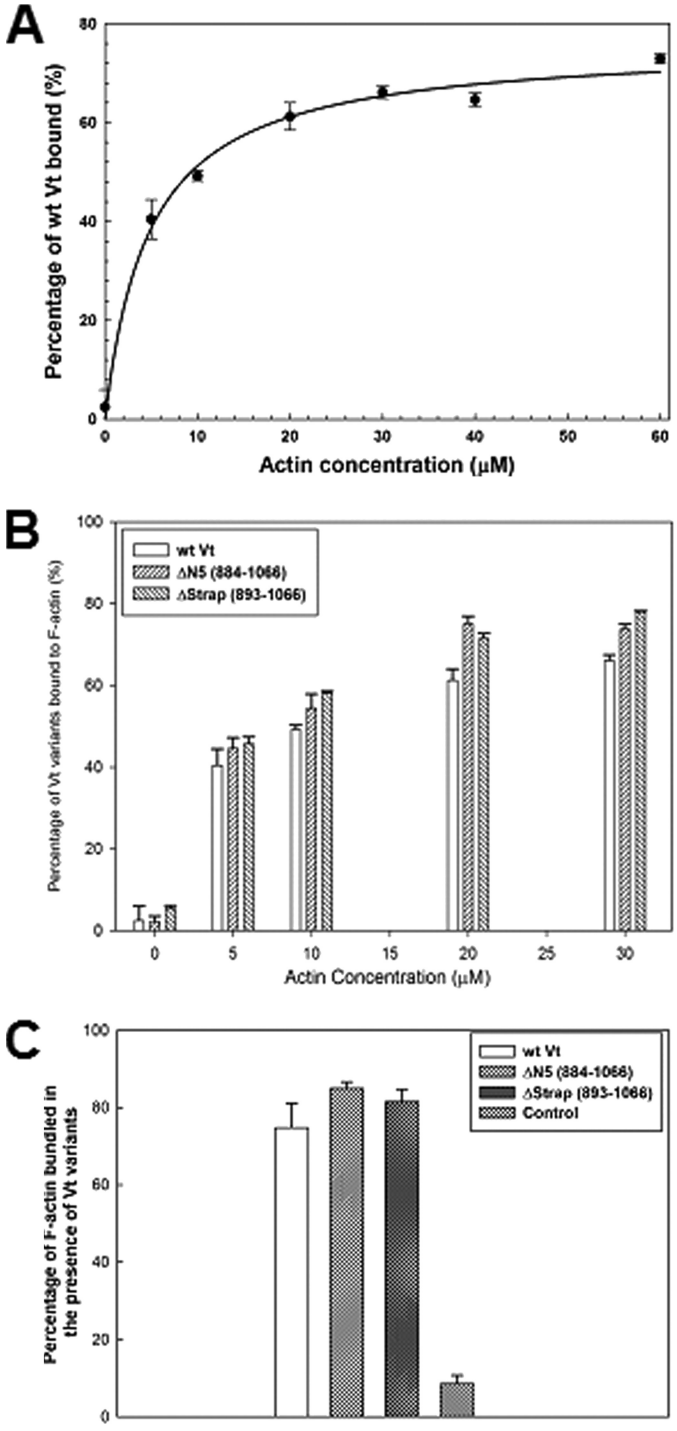

FIGURE 1. **Vt NT deletions within the strap do not affect actin binding and bundling.** *A*, binding of WT Vt to F-actin at actin concentrations ranging from 0 to 60 μM. The *solid line* provides visual guidance; binding to F-actin reaches a plateau at actin concentrations of ~20 μM or higher; WT Vt concentration, 10 μM; *B*, compared with WT Vt, both the ΔN5 and Δstrap Vt variants show slightly enhanced actin binding. Vt variant concentration was 10 μM; actin concentration was 0–30 μM. *C*, Vt variants with partial (ΔN5) and complete deletion of the strap (Δ*strap*) show comparable actin bundling to that of WT Vt. Vt variant concentration was 10 μM; actin concentration was, 20 μM.

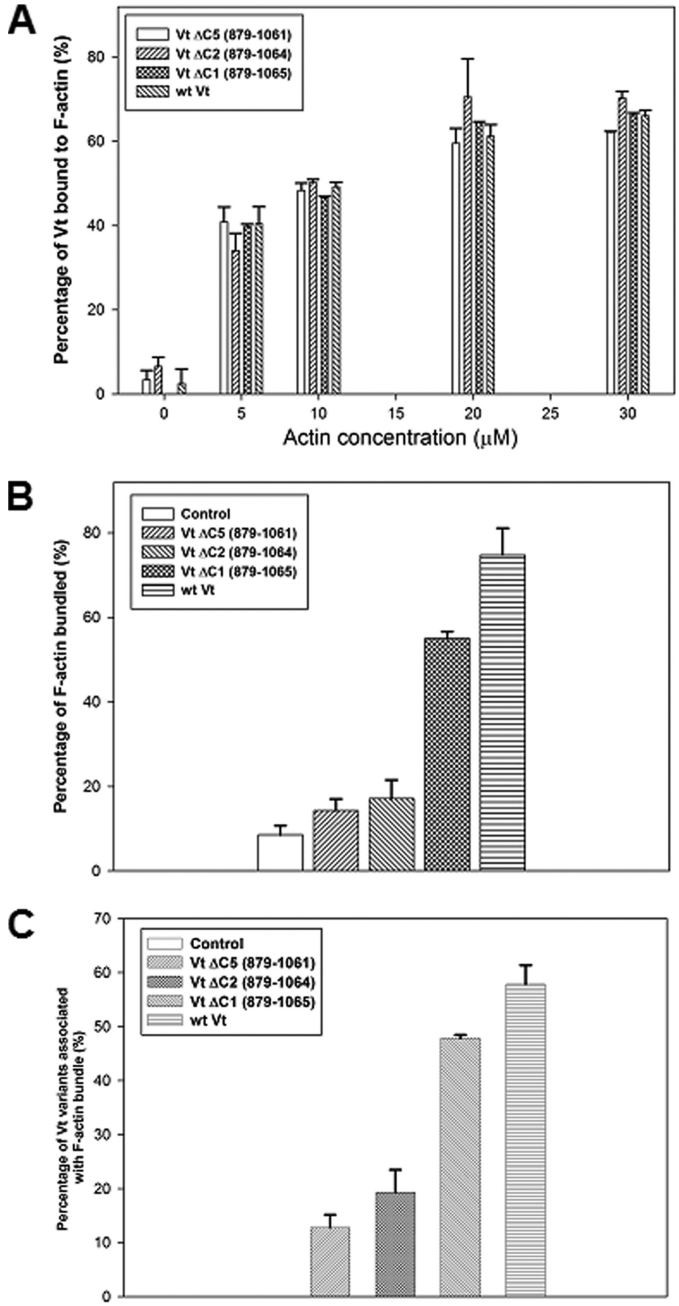

FIGURE 2. **Vinculin CT hairpin is critical for bundling F-actin, but not for binding F-actin.** *A*, compared with WT Vt, Vt variants containing deletions of residues within the CT hairpin does not alter binding to F-actin. Vt variant concentration used was 10 μM; actin concentrations ranged from 0 to 30 μM; *B*, deletion of C-terminal residues 1062 to 1066 (Vt ΔC5) impairs Vt-induced F-actin bundling. Vt concentration was 10 μM; actin concentration was 20 μM. Vt protein was not present in the control runs; *C*, deletion within the Vt C-terminal hairpin reduces the amount of Vt associated with F-actin bundles. Vt concentration was 10 μM; actin concentration was 20 μM. In the absence of Vt, a protein band at ~23 kDa was not observed in the control run.

As shown in Fig. 2*A*, the CT deletion variants, Vt ΔC5(879–1061), Vt ΔC2(879–1064), and Vt ΔC1(879–1065), showed similar actin binding relative to WT Vt, over an A/V ratio range of 0.5 to 3. These results indicate that smaller (5 amino acids or less) amino acid deletions of the Vt C terminus do not alter actin binding to Vt. We then compared the ability of these deletion variants to bundle actin filaments. These analyses were conducted at an A/V ratio of 2 where WT Vt and the deletion variants show close to maximum actin binding. Our findings indicate that all three C-terminal deletion variants impair the ability of Vt to form actin bundles. As shown in Fig. 2*B*, removal

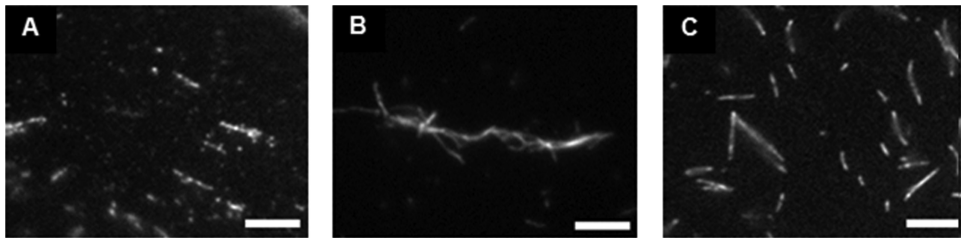

FIGURE 3. **Visualization of actin bundles in the presence and absence of WT Vt and Vt ΔC5 using fluorescence microscopy.** Removal of the CT hairpin significantly impairs F-actin bundling. *A*, in the absence of Vt, only F-actin fragments are observed; *B*, when incubated with WT Vt, F-actin forms thick and stable actin bundles; *C*, upon incubation with Vt ΔC5, F-actin forms randomly oriented thin fragments, similar to those observed in *A*. Samples were prepared using the procedure described for the actin bundling assay. The nominal actin and Vt concentrations during image acquisition are 50 and 25 nM, respectively. *Scale bar*, 25 μm.

of 1 residue (Gln-1066) from the Vt C terminus significantly reduces the percentage of bundled F-actin down from 75 to 55%. Removal of a second amino acid, Tyr-1065, from Vt results in an even more dramatic reduction in actin bundling to 17%, which corresponds to a 77% drop in bundling relative to WT Vt. Further deletion of the entire hairpin (Vt ΔC5) leads to an additional decrease in bundling F-actin down to 14%. In the absence of Vt, we observe that ~10% of actin is bundled in our control samples (Fig. 2*B*). Quantification of Vt variants associated with bundles of actin filaments reveal that the amount of Vt variants associated with F-actin bundles (Fig. 2*C*) correlates with the amount of actin bundles observed in Fig. 2*B*. For example, deletion of CT hairpin (Vt ΔC5) leads to ~78% reduction in Vt associated with F-actin bundles, whereas the amount of F-actin bundles decreases by 81%. As removal of the CT hairpin severely attenuates actin bundling properties of Vt but does not affect actin binding, the Vt CT hairpin appears to play a critical role in bundling actin.

We further examined the role of the Vt CT hairpin in bundling F-actin by fluorescence microscopy. As shown in Fig. 3*A*, few actin bundles are observed for pre-polymerized actin in the absence of WT Vt. However, in the presence of WT Vt (Fig. 3*B*), most actin filaments are incorporated into thick actin bundles at the A/V ratio of 2. These observations agree well with our actin bundling assay results, indicating that ~80% of the actin filaments form bundles. However, removal of the CT hairpin from Vt impairs Vt-mediated actin bundling, as shown by the significant reduction in actin filament bundles observed for Vt ΔC5 relative to WT Vt (Fig. 3*C*). Only randomly oriented thin F-actin fragments are observed, corresponding to a small percentage of actin bundles (~ 14%) (Fig. 2*B*). Both actin co-sedimentation assay results and the fluorescence micrograph analyses suggest that the Vt CT hairpin plays an indispensable role in bundling F-actin.

Vt CT Deletion within the Hairpin Does Not Alter Vt Conformation—We previously conducted NMR and CD analyses on a CT deletion variant (Vt ΔC5) of Vt that lacks the hairpin (34). Results from these studies indicated that loss of 5 amino acids from the Vt CT does not alter the structural integrity of the helix bundle. However, results shown in Fig. 2*B* indicate that amino acids in the CT hairpin play an important role in the ability of Vt to bundle F-actin filaments, as Vt ΔC1, Vt ΔC2, and Vt ΔC5 have significantly impaired actin bundling abilities compared with WT Vt, with Vt ΔC2 possessing similar bundling efficiency to Vt ΔC5. Although our previous NMR studies suggested that Vt ΔC5 does not alter the structural integrity of Vt (34), given the dramatic drop in actin bundling properties associated with both the Vt ΔC2 and Vt ΔC5 variants, we wanted to further compare NMR spectra of Vt ΔC2 and Vt ΔC5 with that of WT Vt. Two-dimensional ^{1}H-^{15}N HSQC NMR spectra are often employed to examine whether mutations or deletions within proteins produce localized or global perturbations by comparison of NH chemical shifts between the WT and mutant protein, as each amino acid with the exception of proline contains a backbone amide that can be used as a site-specific probe. Perturbation of an amides backbone chemical environment will alter its chemical shift as reflected by a change in resonance position within the HSQC spectrum. Moreover, changes in peak intensity and/or line width often reflect alterations in protein dynamic properties. If large scale perturbations in the chemical shifts and/or intensities of the NH peaks are observed, this can indicate that a mutation alters the structural or dynamic properties of the protein, but quantification and verification require additional experiments. We have previously obtained backbone NMR resonance assignments of Vt (37), and demonstrated that the ^{1}H-^{15}N HSQC two-dimensional NMR spectrum of the Vt ΔC5 variant overlays well with WT Vt (34), indicating that deletion of the C terminus does not alter the structural integrity of the helix bundle fold. It is therefore not surprising that the two-dimensional ^{1}H-^{15}N HSQC spectrum of the Vt ΔC2 mutant also overlays quite well with WT Vt (Fig. 4*A*), further supporting our earlier observations that deletions within the hairpin do not alter the helix bundle fold of Vt. Although most amide resonances do not change upon CT hairpin deletion (Vt ΔC5), chemical shift changes are observed for residues proximal to the deletion. Small NH chemical shift changes are observed in the HSQC spectrum of Vt ΔC2 compared with WT Vt for Lys-915, which is located in the loop between helix 1 and 2, Met-930 in helix 2, and Lys-1035 in helix 5. We postulate that these differences are due to removal of Tyr-1065 in the context of Vt ΔC2. Tyr-1065 in the CT hairpin has a number of contacts with helix 2 (*e.g.* K924) and with the loop between helices 1 and 2 (*e.g.* S914) (PDB code 1ST6). Additionally, residues on helix 5 form salt bridges with their counterparts on helix 2 (*e.g.* Arg-1039 on helix 5 and Glu-908 on helix 1) (11). Thus, removal of Tyr-1065 may alter the chemical environment of residues on helices 1 and 2, especially those close to the CT, and subsequently, helix 5. The chemical shift changes observed for Lys-915, Met-930, and Lys-1035 in Vt ΔC2 may indicate that residues proximal to

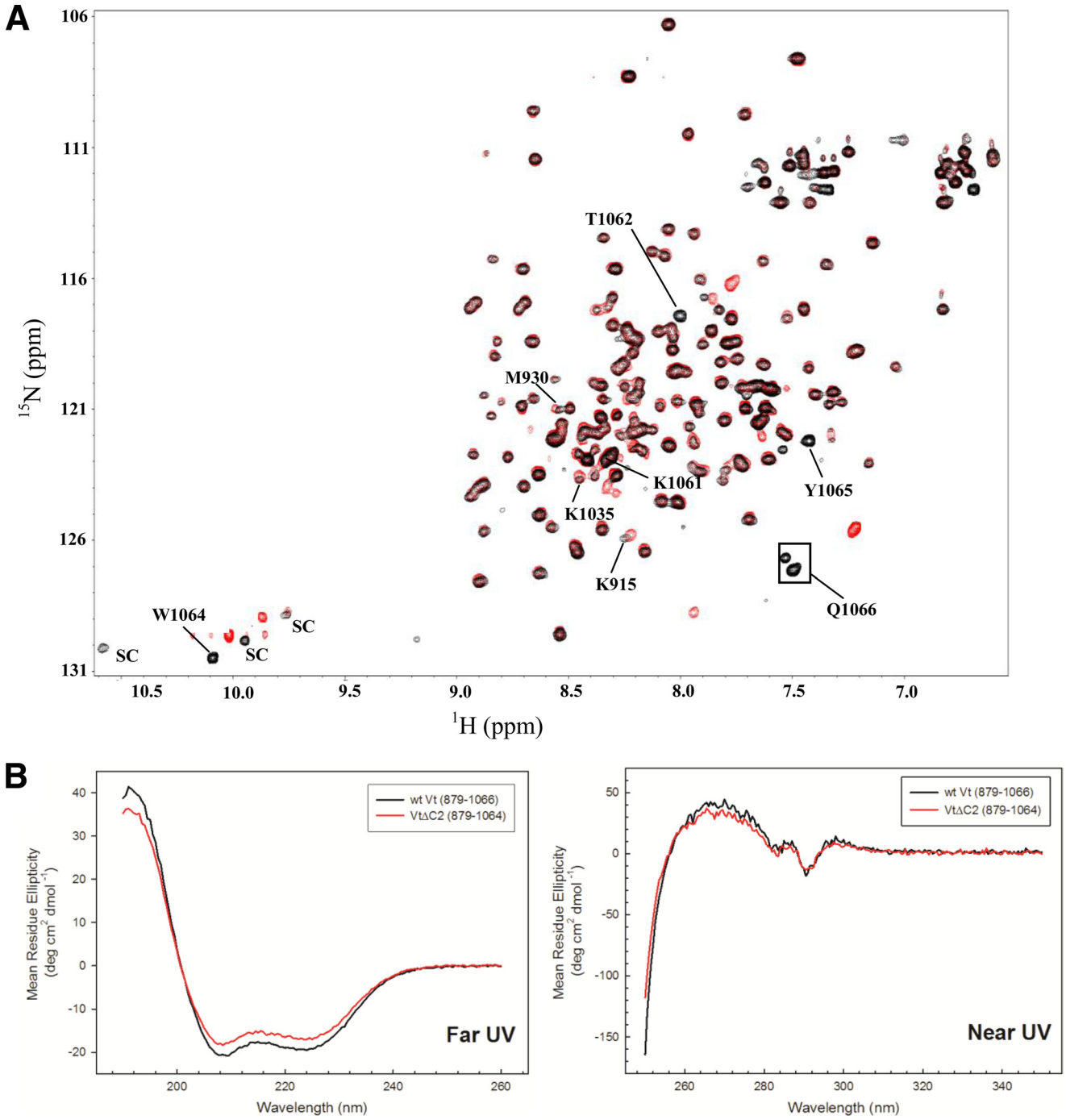

FIGURE 4. **Removal of residues within the Vt C-terminal hairpin does not alter Vt conformation.** *A*, two-dimensional ^{1}H-^{15}N HSQC spectral overlay of WT Vt (*black*) and Vt ΔC2 (*red*). Note that Thr-1062 and Trp-1064 resonances show significant chemical shift changes, whereas Lys-915, Met-930, and Lys-1035 show slight chemical perturbations (within a line width). *SC*, side chain. The weak resonance associated with Gln-1066 represents its minor conformation. *B*, CD spectra overlay of WT Vt (*black*) and Vt ΔC2 (*red*). *Left panel*, far UV; *right panel*, near UV.

the CT deletion site (Thr-1062 through Trp-1064) may be needed for propagation of chemical shift changes to these residues (Fig. 4*A*). The Pro-1063 NH resonance is unobservable in the HSQC spectrum as it lacks a backbone amide.

To corroborate our NMR data, we also acquired CD spectra on WT Vt and Vt ΔC2 (Fig. 4*B*). Both far and near UV spectra of WT Vt and Vt ΔC2 overlay very well, suggesting that neither the secondary structure nor the tertiary structure of Vt ΔC2 are altered. Among the 3 tryptophan residues (Trp-912, Trp-1058, and Trp-1064) in Vt, Trp-912 located in the loop between helix 1 and 2, packs against Trp-1058 in the C terminus, forming a tertiary interaction (PDB code 1ST6). The near UV CD spectrum is likely dominated by Vt tryptophan residues and does not change upon deletion of the last 2 residues within the CT hairpin, suggesting that this tertiary interaction is unaffected. Therefore, both the NMR and CD data indicate CT deletion within the hairpin does not alter the Vt helix bundle fold.

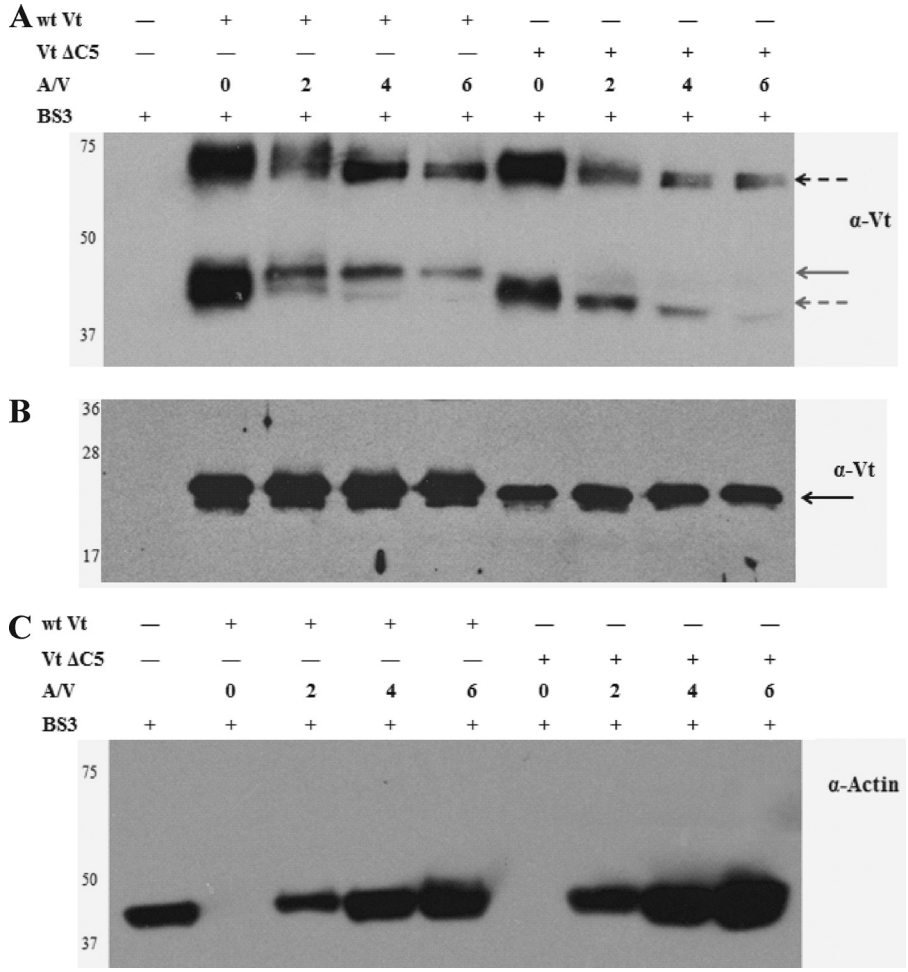

FIGURE 5. **Vt forms a distinct dimer (~45 kDa) in the presence of F-actin.** Cross-linking experiments were conducted at room temperature for 40 min. Final Vt concentration was 2.5 μM; BS3 concentration was 25 μM; Western blots of WT Vt and Vt ΔC5 in the presence of increasing concentrations of actin probed against Vt (*A* and *B*) or actin (*C*). The relative intensity ratio of the lower native dimer band to the upper (actin-induced) dimer band for WT Vt gradually increases when the A/V ratio is raised from 0 to 6. Cross-linking samples were run on SDS-PAGE gels (*B*) to observe the Vt, monomer band (*black arrow*) or Tris acetate 7% gradient gels (*A* and *C*) to observe dimer and trimer species. Although Vt ΔC5 is impaired in actin bundling, a distinct dimer is formed in the presence of actin (lower band, ~40 kDa). The smaller dimer band is distinct in molecular weight and likely differs from the actin-induced dimer that is formed by WT Vt (*C*). *Gray arrows* in both panels indicate the positions of Vt dimer bands (*gray solid arrow* for the actin-induced dimer and the *gray dashed arrow* for the native dimer or a different dimer species in the case of Vt ΔC5). The *black dashed arrow* indicates a Vt trimer species.

Vt Association with F-actin Promotes Vt Dimerization—Vt has a weak propensity to dimerize at submillimolar concentrations (45). However, Johnson and Craig (31) detected formation of a Vt dimer in the presence of F-actin, at concentrations where the native dimer was not observed. They proposed that actin binding to Vt induces a conformational change that exposes a cryptic dimerization site, with dimer formation important for bundling of F-actin filaments. These earlier chemical cross-linking studies were performed using DSS to detect formation of the F-actin-induced Vt dimer. Given our results that removal of the CT hairpin impairs actin bundling but not binding, we postulated that the CT hairpin plays an important role in the formation of the actin-induced Vt dimer. To test this hypothesis, we performed chemical cross-linking studies on WT Vt in the presence and absence of F-actin. Instead of using DSS, which is hydrophobic and requires organic solvents for dissolution in aqueous solution, we employed BS3, the water soluble analog of DSS. Similar to DSS, BS3 forms chemical cross-links with lysine side chains. We first added BS3 to purified WT Vt and incubated the mixture at room temperature for 40 min in the absence of actin. The reaction products were monitored by Western blot analysis using a Vt antibody. In the presence of BS3 (Fig. 5*A*), Vt bands were observed at positions on the gradient gel that correspond to both dimeric and trimeric forms of Vt. Densitometry quantification indicated that the dimer band accounts for ~22% of total Vt in the sample (data not shown). This result was not too surprising, as Vt can dimerize in solution (30, 45), however, with a weak affinity (K_d ~ 360 μM) (45). In fact, a similar dimer contact, which is located at the helix 4/5 interface, was reported (30). Our previous NMR studies revealed that the dimer observed by x-ray crystallography was similar to that observed by us in solution (45), suggesting that the Vt dimer observed in the presence of BS3 corresponds to the dimer observed by both x-ray crystallography and NMR (13, 37, 45). To evaluate whether actin bundling is altered by the presence of BS3, we conducted actin co-sedimentation experiments on WT Vt, Vt ΔC2, and Vt ΔC5, in the absence or presence of a water-soluble cross-linker BS3. As shown in supplemental Fig. S1, the amount of bundled actin is essentially the same in the absence or pres-

ence of BS3, indicating that actin bundling is not artificially enhanced by the use of the cross-linking agent.

We also performed chemical cross-linking experiments in the presence of actin to assess whether the actin-induced dimer was distinct from the native dimer. These experiments were conducted using A/V ratios over the range of 0:1 to 6:1. As shown in supplemental Fig. S3*C*, multiple higher order Vt species form in the absence of actin and the ability for vinculin to form these higher order oligomers has been previously observed (46, 47). Because these higher order Vt oligomers disappear with increasing actin concentrations and because Vt ΔC5 is a F-actin bundling-deficient mutant, we have chosen to focus on changes in the dimer and trimer bands between WT Vt and Vt ΔC5 with increasing concentrations of actin. As shown in Fig. 5*A*, WT Vt forms two distinct dimer bands that are observed in the presence of actin, whereas only one (lower dimer band; native dimer) exists in the absence of actin. These results suggest that the actin-induced Vt dimer is distinct from the native dimer. The relative intensity ratio of the lower "native" dimer band to the upper (actin-induced) dimer band gradually increases when the A/V ratio is raised from 0 to 6, suggesting that in the presence of actin, an actin-induced dimer is favored. One possible explanation for these results is that the native dimer competes with the ability of actin to bind Vt and/or promote formation of the actin-induced Vt dimer. As Vt is completely saturated in the presence of excess actin, few Vt molecules are available to form the native dimer.

Interestingly, we observe a band at ~65 kDa in the absence and presence of actin. However, this band is not observed by Western blot analysis using an anti-actin antibody (supplemental Fig. S3*D*), suggesting that this band corresponds to a trimeric Vt species. Because this band forms in both the absence and presence of actin, it is unclear whether the Vt trimer contributes to F-actin bundling. We do observe that the intensity of the trimer band weakens with increasing actin concentrations. This could possibly be due to saturation of Vt in the presence of excess actin, such that the incidence for native dimer and trimer decreases. This coincides with our observations that with excess actin beyond an A/V ratio of 2:1, bundling efficiency decreases (supplemental Fig. S2).

The most notable difference between WT Vt and Vt ΔC5 occurs at the corresponding dimer band. Because Vt ΔC5 shows significantly lower actin bundling ability relative to WT Vt, we expected that Vt ΔC5 would show a reduction in the Vt dimer observed upon actin binding. The chemical cross-linking results on Vt ΔC5, however, are inconsistent with this prediction. Fig. 5*A* shows that in the presence of actin, a distinct Vt ΔC5 dimer band emerges that is of lower molecular weight than the native dimer. Although this could initially be attributed to a difference in length of the protein, Vt ΔC5 typically is the same molecular weight as WT Vt as shown by the monomer (Fig. 5*B*) and trimer bands (Fig. 5*A*). The lower, actin-induced Vt ΔC5 dimer band decreases in intensity at higher A/V ratios. These results suggest that the lower actin-induced Vt ΔC5 dimer band is distinct from that of WT Vt, possibly due to a more compact conformation, and is likely the reason why Vt ΔC5 does not bundle F-actin efficiently.

Vinculin CT Deletion Affects Cell Adhesion—To explore the role of the vinculin CT hairpin during cell adhesion, vinculin knock-out murine embryo fibroblasts ($Vin^{-/-}$ MEFs) were transfected with GFP-tagged WT vinculin or a CT hairpin deletion mutant (ΔC5). In $Vin^{-/-}$ MEFs, the transfection efficiencies and expression levels of WT and ΔC5 vinculin as determined by immunoblots were identical (data not shown). When plated onto FN, $Vin^{-/-}$ MEFs expressing the ΔC5 mutant were less spread than cells expressing full-length WT vinculin (Fig. 6, *A* and *C*). The average cell area was 1,270 ± 134 μm^2 (mean ± S.E.) for the ΔC5-expressing cells and 1,968 ± 200 μm^2 for the WT (Fig. 6*C*). We also observed that the $Vin^{-/-}$ MEFs transfected with the ΔC5 mutant formed fewer than half of the focal adhesions (FA) (79 FAs/cell as median value) than cells transfected with WT vinculin (191 FAs/cell as median value) (Fig. 6*B*). In cells expressing ΔC5 vinculin, the decrease in FAs number was associated with a slight increase in adhesion size (39%) compared with cells expressing WT vinculin (Fig. 6*C*). However, the difference in adhesion size was not statistically significant ($p = 0.22$).

The Vinculin CT Hairpin Is Necessary for the Mechanical Response to Force on Integrins—Applying force on FAs either by cell-generated tension or external forces has been shown to trigger local stiffening in cells, also called reinforcement, which has been shown to be central to many aspects of cell biology. Vinculin has been demonstrated to play an important role in force transduction (48, 49). To determine whether the CT hairpin of vinculin contributes to the stiffening response to force on integrins, we used magnetic tweezers to apply a controlled force on magnetic beads coated with FN. The local viscoelastic properties of the cells were determined by measuring bead displacements due to a known force induced by a magnetic field (50). We observed that the basal stiffness of $Vin^{-/-}$ MEFs transfected with ΔC5 vinculin was not significantly different from $Vin^{-/-}$ MEFs transfected with WT vinculin (2.6 *versus* 2.2 pascals) (Fig. 7*A*). When pulses of constant force were applied, we measured a local increase in spring constant of the $Vin^{-/-}$ MEFs transfected with WT vinculin (48% after the second pulse) (Fig. 7*B*). However, cells expressing the ΔC5 vinculin lost this stiffening response following force application (Fig. 7*B*).

DISCUSSION

Vinculin has been implicated in cell morphology and adhesion turnover as $Vin^{-/-}$ MEFs possess a less adherent, round morphology and increased motility (6, 11). Vinculin is also believed to play a critical role in sensing and transducing force. Interactions between actin and vinculin are believed to be critical for the functional properties of vinculin, but the role of this interaction in regulation of cell morphology, motility, and force transduction is poorly understood. Models for how vinculin binds and bundles actin have been proposed. One common feature of these models is that the tail domain of vinculin binds to F-actin through two distinct binding sites, with F-actin binding promoting a cryptic dimerization site on Vt that facilitates cross-linking of actin filaments (31, 32). In this study, we examined the role of the Vt NT strap and CT hairpin in actin binding and bundling. Removal of the Vt NT strap slightly increases its actin binding. However, in contrast to earlier observations (32),

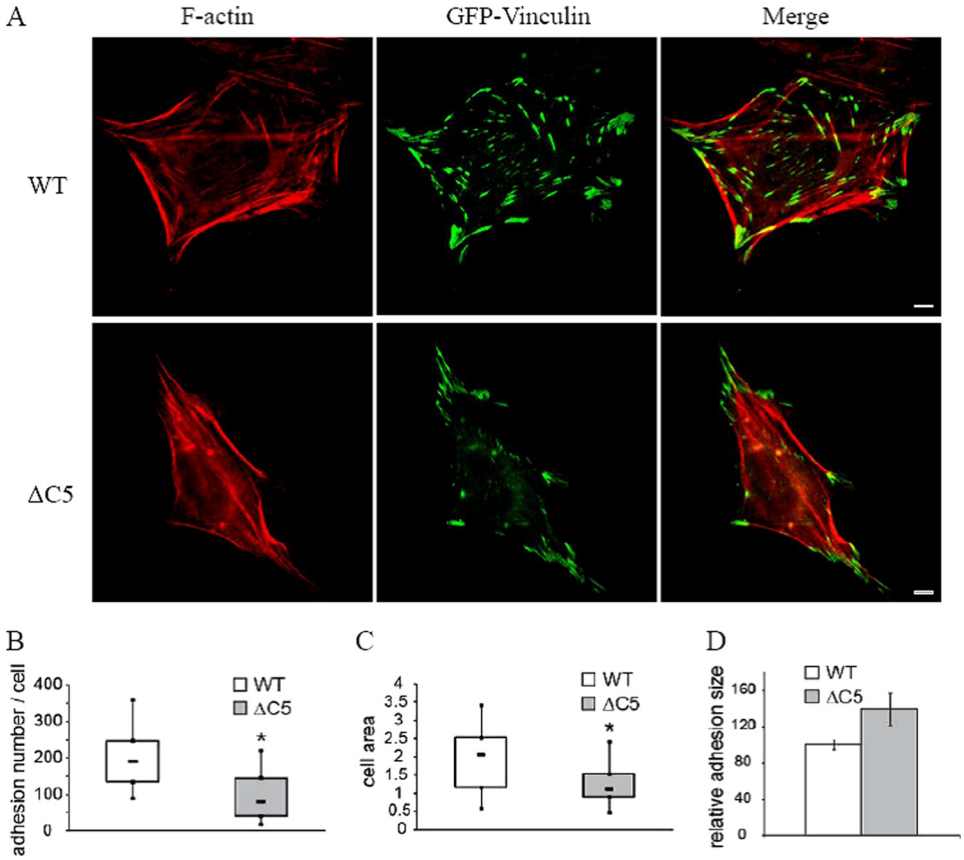

FIGURE 6. **Vt CT hairpin deletion affects cell adhesion.** *A*, Vin$^{-/-}$ MEFs were transfected with WT or ΔC5 vinculin and plated on FN. After fixation, F-actin and FAs were stained using phalloidin and GFP-tagged vinculin variants, respectively. *Scale bar* is 25 μm. *B–D*, adhesion number per cell (*B*), cell area (*C*), and adhesion size (*D*) were analyzed ($n = 19$; *, $p < 0.01$). Box plots indicate median values and capture 50% of data in *boxes* and 80% in the *lines*.

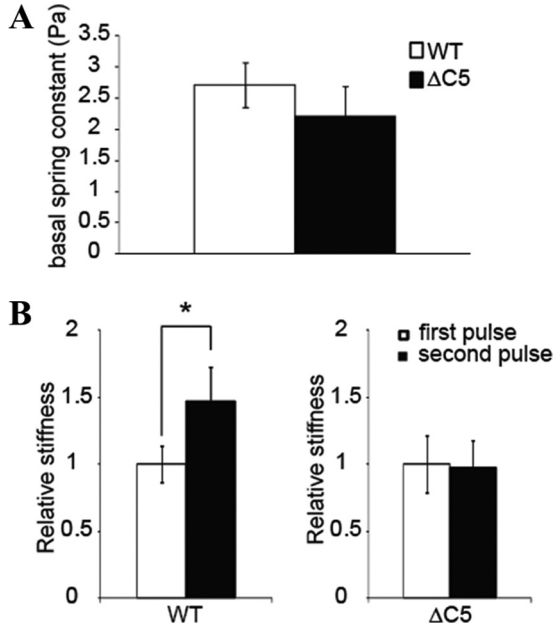

FIGURE 7. **The Vt CT hairpin is necessary for the mechanical response to force on integrins.** *a*, within measurement errors, WT vinculin and ΔC5 vinculin have comparable basal stiffness. Spring constant was calculated for the first pulse of force applied to FN-coated beads bound to Vin$^{-/-}$ MEFs transfected with WT or ΔC5 vinculin ($n = 15$). *b*, upon applying pulses of a constant force, relative stiffness of Vin$^{-/-}$ MEFs transfected with WT vinculin increases, whereas the stiffness of Vin$^{-/-}$ MEFs transfected with ΔC5 vinculin does not change within errors. For the relative stiffness measurements, two force pulses were applied to FN-coated beads bound to Vin$^{-/-}$ MEFs transfected with either WT or ΔC5 vinculin ($n = 15$).

we report here that the Vt CT hairpin, rather than the NT strap region, is indispensable for F-actin bundling. In particular, removal of the CT hairpin results in a significant loss of actin bundling, not actin binding, which may result from the formation of an actin-induced Vt dimer that is unable to cross-link actin filaments or possibly functional differences associated with higher order oligomers. We also observe that loss of the CT hairpin leads to reduced adhesion number, decreased cell spreading, and impaired cell stiffness responses upon applied force, suggesting that the CT hairpin plays an important role in adhesion formation and cell mechanical responses.

Regulatory Role of the Vt CT Hairpin in F-actin Bundling—Results from our studies indicate that removal of the Vt CT hairpin maintains actin binding but shows significantly impaired actin bundling, whereas removal of the Vt NT strap is dispensable for both actin binding and bundling. We characterized three small CT hairpin deletion variants of Vt, namely Vt ΔC1, Vt ΔC2, and Vt ΔC5. All three Vt variants showed impaired bundling and reduced association of Vt with F-actin bundles, indicating that the Vt CT hairpin structure affects formation and/or function of the actin-induced Vt dimer. As F-actin binding to Vt has been proposed to expose a dimerization site in Vt important for cross-linking of F-actin filaments, we performed chemical cross-linking studies to monitor formation of the Vt dimer in the presence and absence of actin. Results from these studies indicate that the Vt dimer formed in the presence of F-actin is distinct from native Vt dimer

observed previously by x-ray crystallography and NMR (30, 45). Moreover, the F-actin-induced Vt dimer appears to compete with the native Vt dimer, suggesting that F-actin binding or bundling interferes with formation of the native Vt dimer (Fig. 5*A* and supplemental Fig. S3). Although it is somewhat surprising that the actin-induced Vt dimer bands are present for the Vt ΔC5 variant (Fig. 5*A*, *lower dimer band*) at comparable levels to that of WT Vt, the dimer that is formed runs at a lower molecular weight, possibly indicating a more tightly packed conformation. Given that there is a 78% reduction in Vt ΔC5 associated with F-actin bundles, the actin-induced Vt dimer or trimer may not be competent to induce bundling of actin filaments, possibly due to geometric constraints. We carefully optimized the cross-linker concentration to detect the actin-induced Vt oligomers while reducing nonspecific cross-linking reactions. Under these conditions, we expect to see an excess of monomeric Vt, as previously reported (31). We also observe a decrease in the intensity of dimer and trimer bands for both WT Vt and Vt ΔC5 at higher A/V ratios. We speculate (as illustrated in Fig. 8) that this is due to a reduction in the total number of Vt oligomer species that is able to properly form, resulting in a reduction in the number of bundled actin filaments. Although we also see a significant population of the Vt monomer remaining, it has been previously observed that not all the Vt monomer will be incorporated into a dimer even when high amounts of a cross-linking agent are used (31). However, at lower concentrations similar to the amount used in this study, both monomer and dimer bands will be observed. Additionally, because actin can also be cross-linked and we use high A/V ratios in this study, it is possible that excess actin reacts with the cross-linker and contributes to the decrease in the dimer and trimer intensity we observe (supplemental Fig. 3*D*). By using a lower concentration of the cross-linking agent, we are able to differentiate between dimer and/or higher order oligomers that form specifically in the presence of actin. Previous results have indicated that Vt optimally binds to F-actin through two binding sites at an A/V ratio of 2:1 (31, 32). Consistent with this model, our data shows optimal actin bundling occurs at an A/V ratio of ~2:1 with bundling efficiency decreasing at high A/V ratios (supplemental Fig. S2). Based on these observations, we postulate that when actin is in excess, Vt is not uniformly distributed along each filament to efficiently bundle F-actin, or rather, there is a lack in reinforcement by Vt to stably bundle actin filaments. Although we cannot distinguish whether the Vt oligomer responsible for bundling is a dimer or a trimer, we only observe differences between WT Vt and the bundling-deficient Vt ΔC5 variant, with the dimer and not the trimer bands. We are currently pursuing studies to characterize the actin-induced Vt dimer and trimer structures derived from WT Vt and CT deletion variants.

Vinculin CT Hairpin Affects Focal Adhesion Properties—We also demonstrate that when ΔC5 vinculin is expressed in $Vin^{-/-}$ cells, the cells have fewer, slightly larger adhesions in comparison to WT vinculin (Fig. 6, *B* and *D*). In addition, cells expressing ΔC5 are smaller than cells expressing WT vinculin (Fig. 6*C*). Considering the bundling deficiencies of Vt ΔC5 observed *in vitro*, cells expressing this mutant might be expected to have smaller and less stable adhesions related to possibly enhanced release of bound ΔC5 vinculin from F-actin. However, because this is the first vinculin mutant reported where actin binding is decoupled from its actin bundling capabilities, it is yet to be determined whether the phenotype observed results from the inability of vinculin to cross-link actin filaments and/or other factors. The phenotype observed could be due to overcompensation from other actin-bundling proteins. Alternatively, deletion of the CT hairpin may either alter binding of an interacting molecule that modulates focal adhesion properties or result in formation of weaker adhesions, as supported by our mechanical force data. We plan to explore whether deletion of the CT hairpin alters binding of interaction partner(s) in future studies to discern between these possibilities.

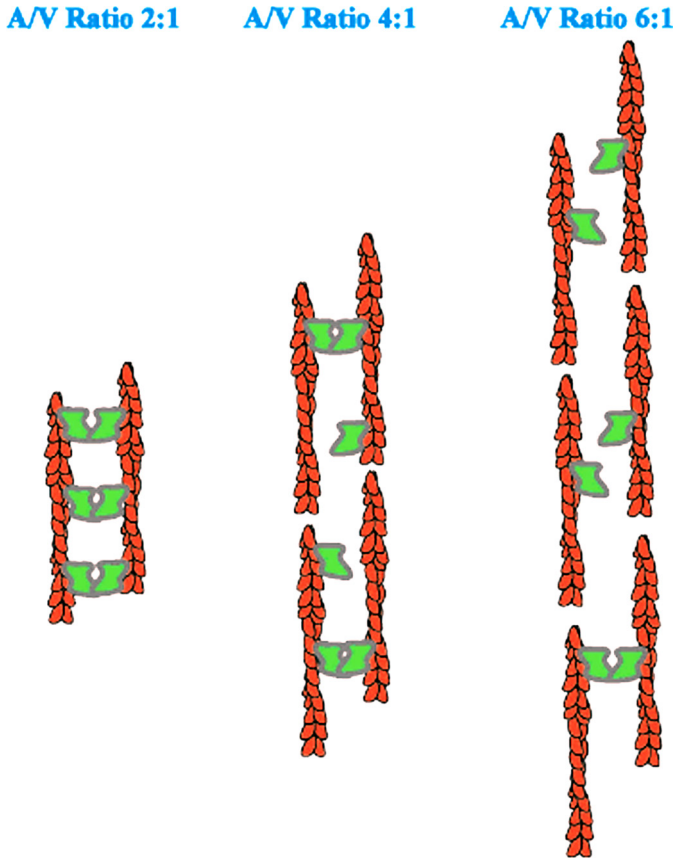

FIGURE 8. **Model for actin-induced vinculin tail oligomerization and bundling of F-actin.** According to our data (see Fig. 1*A* and supplemental Fig. S2) and the dimer model (31, 32), optimal bundling of actin by Vt is expected to occur at an A/V ratio of 2:1, assuming Vt binds to two sites on an F-actin unit and upon binding to actin, Vt dimerizes which in turn promotes bundling of actin. When actin (*red*) is in excess and Vt (*green*) is saturated, the bundling efficiency decreases as shown by our cross-linking data and F-actin bundling saturation curves. We hypothesize that the lack of reinforcement by Vt to bundle F-actin when actin is in excess, results in reduced bundling efficiency as well as formation of actin-induced dimer species.

Vinculin CT Hairpin Contributes to Mechanical Response to Force—Due to its particular localization within the FA (51), vinculin plays a central role in the regulation of cell mechanics and its depletion has been shown to dramatically alter cellular rigidity (52). Force, either internally generated or externally applied, has been shown to trigger the recruitment of vinculin to FA (53, 54), which in turn increases the linkage between actin

cytoskeleton and extracellular matrix (55). The force sensing abilities of vinculin have also been shown to contribute to cell migration and FA stabilization (49). Here, we demonstrate that vinculin CT hairpin deletion does not change the basal stiffness of the cells but prevents cellular stiffening in response to force (Fig. 7). Previous work using a vinculin mutant lacking 15 CT residues similarly found that there was a reduced stiffening response to mechanical force applied to fibronectin-coated beads (56). In that study, it was suggested that differences in the ability of this vinculin mutant to respond to cell mechanical forces were due to loss of its anchorage to lipids. However, our previous studies have demonstrated that deletions beyond the CT hairpin significantly disrupt the structural integrity of Vt and that deletion of the CT hairpin does not alter the ability of the vinculin tail domain to interact with phosphatidylinositol (4,5)-bisphosphate (34). Because the vinculin CT hairpin is critical for actin bundling *in vitro* but not for lipid association, our results suggest that vinculin-dependent actin bundling may strengthen the link between integrin-based adhesion and the actin cytoskeleton in response to force. Other bundling proteins, such as α-actinin (57), have also been suggested to contribute to adhesion reinforcement. However, the fact that vinculin-mediated actin bundling only alters the dynamic stiffening in response to tension and does not impact basal stiffness is surprising. Another possibility is that altered actin bundling may not be the only cause for the absence of the strengthening response observed in cells transfected with the ΔC5 mutant. Adhesion reinforcement requires a complex signaling cascade from mechanosensor stimulation to actin machinery activation and assembly. Vinculin is known to interact with many other FA components (58) and actin cytoskeleton regulators, such as Arp2/3 (20). The CT hairpin could potentially act as a scaffold and contribute to the proper subcellular localization of molecular actors involved in the dynamic cytoskeleton remodeling observed in response to force. Potentially, phosphorylation of Tyr-1065 within the CT hairpin could either affect actin bundling or regulate binding of vinculin toward unknown ligands because Src, the only kinase shown to phosphorylate this residue, has been shown to be activated in response to force. Further work is necessary to elucidate the precise molecular mechanism by which vinculin CT hairpin regulates reinforcement.

Acknowledgments—We thank Dr. Susan Craig for providing a detailed protocol for vinculin cross-linking as well as a Vt antibody. We also thank Dr. Richard Cheney for advice with the fluorescence microscopy of F-actin bundles assay. We thank Dr. Greg Young, the NMR facility manager at University of North Carolina-Chapel Hill, for assistance in NMR data collection, and Dr. Ashutosh Tripathy, Director of the UNC Macromolecular Interactions Facility, for assistance in acquisition of CD spectra. We thank Dr. Min-qi Lu for preparation of monomeric actin.

REFERENCES

1. Janmey, P. A., and McCulloch, C. A. (2007) *Annu. Rev. Biomed. Eng.* **9,** 1–34
2. Parsons, J. T., Horwitz, A. R., and Schwartz, M. A. (2010) *Nat. Rev. Mol. Cell Biol.* **11,** 633–643
3. Geiger, B., Spatz, J. P., and Bershadsky, A. D. (2009) *Nat. Rev. Mol. Cell Biol.* **10,** 21–33
4. Geiger, B., and Bershadsky, A. (2001) *Curr. Opin. Cell Biol.* **13,** 584–592
5. Ziegler, W. H., Liddington, R. C., and Critchley, D. R. (2006) *Trends Cell Biol.* **16,** 453–460
6. Xu, W., Baribault, H., and Adamson, E. D. (1998) *Development* **125,** 327–337
7. Zemljic-Harpf, A. E., Ponrartana, S., Avalos, R. T., Jordan, M. C., Roos, K. P., Dalton, N. D., Phan, V. Q., Adamson, E. D., and Ross, R. S. (2004) *Am. J. Pathol.* **165,** 1033–1044
8. Byrne, B. J., Kaczorowski, Y. J., Coutu, M. D., and Craig, S. W. (1992) *J. Biol. Chem.* **267,** 12845–12850
9. Maeda, M., Holder, E., Lowes, B., Valent, S., and Bies, R. D. (1997) *Circulation* **95,** 17–20
10. Olson, T. M., Illenberger, S., Kishimoto, N. Y., Huttelmaier, S., Keating, M. T., and Jockusch, B. M. (2002) *Circulation* **105,** 431–437
11. Coll, J. L., Ben-Ze'ev, A., Ezzell, R. M., Rodríguez Fernández, J. L., Baribault, H., Oshima, R. G., and Adamson, E. D. (1995) *Proc. Natl. Acad. Sci. U.S.A.* **92,** 9161–9165
12. Subauste, M. C., Pertz, O., Adamson, E. D., Turner, C. E., Junger, S., and Hahn, K. M. (2004) *J. Cell Biol.* **165,** 371–381
13. Bakolitsa, C., Cohen, D. M., Bankston, L. A., Bobkov, A. A., Cadwell, G. W., Jennings, L., Critchley, D. R., Craig, S. W., and Liddington, R. C. (2004) *Nature* **430,** 583–586
14. Johnson, R. P., and Craig, S. W. (1994) *J. Biol. Chem.* **269,** 12611–12619
15. Kroemker, M., Rüdiger, A. H., Jockusch, B. M., and Rüdiger, M. (1994) *FEBS Lett.* **355,** 259–262
16. Weiss, E. E., Kroemker, M., Rüdiger, A. H., Jockusch, B. M., and Rüdiger, M. (1998) *J. Cell Biol.* **141,** 755–764
17. Brindle, N. P., Holt, M. R., Davies, J. E., Price, C. J., and Critchley, D. R. (1996) *Biochem. J.* **318,** 753–757
18. Kioka, N., Sakata, S., Kawauchi, T., Amachi, T., Akiyama, S. K., Okazaki, K., Yaen, C., Yamada, K. M., and Aota, S. (1999) *J. Cell Biol.* **144,** 59–69
19. Mandai, K., Nakanishi, H., Satoh, A., Takahashi, K., Satoh, K., Nishioka, H., Mizoguchi, A., and Takai, Y. (1999) *J. Cell Biol.* **144,** 1001–1017
20. DeMali, K. A., Barlow, C. A., and Burridge, K. (2002) *J. Cell Biol.* **159,** 881–891
21. Wood, C. K., Turner, C. E., Jackson, P., and Critchley, D. R. (1994) *J. Cell Sci.* **107,** 709–717
22. Hüttelmaier, S., Bubeck, P., Rüdiger, M., and Jockusch, B. M. (1997) *Eur. J. Biochem.* **247,** 1136–1142
23. Johnson, R. P., Niggli, V., Durrer, P., and Craig, S. W. (1998) *Biochemistry* **37,** 10211–10222
24. Gilmore, A. P., and Burridge, K. (1996) *Nature* **381,** 531–535
25. Weekes, J., Barry, S. T., and Critchley, D. R. (1996) *Biochem. J.* **314,** 827–832
26. Cohen, D. M., Chen, H., Johnson, R. P., Choudhury, B., and Craig, S. W. (2005) *J. Biol. Chem.* **280,** 17109–17117
27. Chen, H., Choudhury, D. M., and Craig, S. W. (2006) *J. Biol. Chem.* **281,** 40389–40398
28. Cohen, D. M., Kutscher, B., Chen, H., Murphy, D. B., and Craig, S. W. (2006) *J. Biol. Chem.* **281,** 16006–16015
29. Borgon, R. A., Vonrhein, C., Bricogne, G., Bois, P. R., and Izard, T. (2004) *Structure* **12,** 1189–1197
30. Bakolitsa, C., de Pereda, J. M., Bagshaw, C. R., Critchley, D. R., and Liddington, R. C. (1999) *Cell* **99,** 603–613
31. Johnson, R. P., and Craig, S. W. (2000) *J. Biol. Chem.* **275,** 95–105
32. Janssen, M. E., Kim, E., Liu, H., Fujimoto, L. M., Bobkov, A., Volkmann, N., and Hanein, D. (2006) *Mol. Cell* **21,** 271–281
33. Saunders, R. M., Holt, M. R., Jennings, L., Sutton, D. H., Barsukov, I. L., Bobkov, A., Liddington, R. C., Adamson, E. A., Dunn, G. A., and Critchley, D. R. (2006) *Eur. J. Biochem.* **85,** 487–500
34. Palmer, S. M., Playford, M. P., Craig, S. W., Schaller, M. D., and Campbell, S. L. (2009) *J. Biol. Chem.* **284,** 7223–7231
35. Fisher, J. K., Cribb, J., Desai, K. V., Vicci, L., Wilde, B., Keller, K., Taylor, R. M., Haase, J., Bloom, K., O'Brien, E. T., and Superfine, R. (2006) *Rev. Sci. Instrum.* **77,** nihms8302
36. Dixon, R. D., Arneman, D. K., Rachlin, A. S., Sundaresan, N. R., Costello, M. J., Campbell, S. L., and Otey, C. A. (2008) *J. Biol. Chem.* **283,** 6222–6231
37. Palmer, S. M., and Campbell, S. L. (2008) *Biomol. NMR Assign.* **2,** 69–71
38. Delaglio, F., Grzesiek, S., Vuister, G. W., Zhu, G., Pfeifer, J., and Bax, A.

(1995) *J. Biomol. NMR* **6,** 277–293
39. Johnson, B. A., and Blevins, R. A. (1994) *J. Biomol. NMR* **4,** 603–614
40. Zamir, E., Katz, B. Z., Aota, S., Yamada, K. M., Geiger, B., and Kam, Z. (1999) *J. Cell Sci.* **112,** 1655–1669
41. Berginski, M. E., Vitriol, E. A., Hahn, K. M., and Gomez, S. M. (2011) *PLoS One* **6,** e22025
42. Bausch, A. R., Möller, W., and Sackmann, E. (1999) *Biophys. J.* **76,** 573–579
43. Thoumine, O., and Ott, A. (1997) *J. Cell Sci.* **110,** 2109–2116
44. Wen, K. K., Rubenstein, P. A., and DeMali, K. A. (2009) *J. Biol. Chem.* **284,** 30463–30473
45. Palmer, S. M., Schaller, M. D., and Campbell, S. L. (2008) *Biochemistry* **47,** 12467–12475
46. Molony, L., and Burridge, K. (1985) *J. Cell Biochem.* **29,** 31–36
47. Winkler, J., Lünsdorf, H., and Jockusch, B. M. (1996) *J. Struct. Biol.* **116,** 270–277
48. Ji, L., Lim, J., and Danuser, G. (2008) *Nat. Cell Biol.* **10,** 1393–4000
49. Grashoff, C., Hoffman, B. D., Brenner, M. D., Zhou, R., Parsons, M., Yang, M. T., McLean, M. A., Sligar, S. G., Chen, C. S., Ha, T., and Schwartz, M. A. (2010) *Nature* **466,** 263–266
50. O'Brien, E. T., Cribb, J., Marshburn, D., Taylor, R. M., and Superfine, R. (2008) in *Biophysical Tools for Biologists, In Vivo Techniques*, Vol. 2, pp. 433–450, Elsevier Academic Press Inc., San Diego
51. Kanchanawong, P., Shtengel, G., Pasapera, A. M., Ramko, E. B., Davidson, M. W., Hess, H. F., and Waterman, C. M. (2010) *Nature* **468,** 580–584
52. Goldmann, W. H., Galneder, R., Ludwig, M., Xu, W., Adamson, E. D., Wang, N., and Ezzell, R. M. (1998) *Exp. Cell Res.* **239,** 235–242
53. Pasapera, A. M., Schneider, I. C., Rericha, E., Schlaepfer, D. D., and Waterman, C. M. (2010) *J. Cell Biol.* **188,** 877–890
54. Galbraith, C. G., Yamada, K. M., and Sheetz, M. P. (2002) *J. Cell Biol.* **159,** 695–705
55. Schwartz, M. A. (2009) *Science* **323,** 588–589
56. Diez, G., Kollmannsberger, P., Mierke, C. T., Koch, T. M., Vali, H., Fabry, B., and Goldmann, W. H. (2009) *Biophys. J.* **97,** 3105–3112
57. von Wichert, G., Haimovich, B., Feng, G. S., and Sheetz, M. P. (2003) *EMBO J.* **22,** 5023–5035
58. Carisey, A., and Ballestrem, C. (2011) *Eur. J. Cell Biol.* **90,** 157–163